AGU PUBLICATIONS

Geophysical Research Letters

RESEARCH LETTER

10.1002/2015GL066641

Key Points:
- Slowdown in isoprene chemistry due to chemistry-turbulence interactions
- Smaller differences between modeled and observed OH densities than in previous studies

Supporting Information:
- Texts S1–S7, Figures S1–S11, and Tables S1 and S2

Correspondence to:
T. Karl,
thomas.Karl@uibk.ac.at

Citation:
Kaser, L., et al. (2015), Chemistry-turbulence interactions and mesoscale variability influence the cleansing efficiency of the atmosphere, *Geophys. Res. Lett.*, *42*, 10,894–10,903, doi:10.1002/2015GL066641.

Received 20 OCT 2015
Accepted 16 NOV 2015
Accepted article online 24 NOV 2015
Published online 19 DEC 2015

Chemistry-turbulence interactions and mesoscale variability influence the cleansing efficiency of the atmosphere

L. Kaser[1], T. Karl[2], B. Yuan[3,4], R. L. Mauldin III[5,6], C. A. Cantrell[5], A. B. Guenther[7], E. G. Patton[1], A. J. Weinheimer[1], C. Knote[1,8], J. Orlando[1], L. Emmons[1], E. Apel[1], R. Hornbrook[1], S. Shertz[1], K. Ullmann[1], S. Hall[1], M. Graus[3,9], J. de Gouw[3,4], X. Zhou[10], and C. Ye[10]

[1]National Center for Atmospheric Research, Boulder, Colorado, USA, [2]Institute of Atmospheric and Cryospheric Sciences, University of Innsbruck, Innsbruck, Austria, [3]Chemical Sciences Division, NOAA Earth System Research Laboratory, Boulder, Colorado, USA, [4]Cooperative Institute for Research in Environmental Sciences, University of Colorado Boulder, Boulder, Colorado, USA, [5]Department of Atmospheric and Oceanic Sciences, University of Colorado Boulder, Boulder, Colorado, USA, [6]Department of Physics, University of Helsinki, Helsinki, Finland, [7]Pacific Northwest National Laboratory, Richland, Washington, USA, [8]Now at Experimental Meteorology, Faculty of Physics, Ludwig Maximilian University of Munich, Munich, Germany, [9]Now at Institute of Atmospheric and Cryospheric Sciences, University of Innsbruck, Innsbruck, Austria, [10]New York State Department of Health, Wadsworth Center, Albany, New York, USA

Abstract The hydroxyl radical (OH) is the most important oxidant in the atmosphere and the primary sink for isoprene, the dominant volatile organic compound emitted by vegetation. Recent research on the atmospheric oxidation capacity in isoprene-dominated environments has suggested missing radical sources leading to significant overestimation of the lifetime of isoprene. Here we report, for the first time, a comprehensive experimental budget of isoprene in the planetary boundary layer based on airborne flux measurements along with in situ OH observations in the Southeast and Central U.S. Our findings show that surface heterogeneity of isoprene emissions lead to a physical separation of isoprene and OH resulting in an effective slowdown in the chemistry. Depending on surface heterogeneity, the intensity of segregation (I_s) could locally slow down isoprene chemistry up to 30%. The effect of segregated reactants in the planetary boundary layer on average has an influence on modeled OH radicals that is comparable to that of recently proposed radical recycling mechanisms.

1. Introduction

Forests emit a vast range of nonmethane volatile organic compounds (NMVOC) that are linked to carbon metabolism and different critical functions such as plant signaling and protection from pathogens [*Loreto et al.,* 2014]. It is now estimated that NMVOC emitted from forests account for about 70–90% of the global budget (1300 TgC/yr) [*Goldstein and Galbally*, 2007]. Isoprene production dominates biogenic NMVOC emissions, totaling about 550 TgC/yr [*Guenther et al.,* 2006], an emission rate, which is comparable to the global emission flux of methane into the atmosphere.

Oxidation and subsequent removal of these reduced carbon species via dry and wet deposition are among the most important processes that prevent their accumulation. In the lower atmosphere, the atmosphere's cleansing efficiency is initiated by the OH radical formed by the photolysis of ozone followed by reaction of excited oxygen atoms with water vapor. This leads to the formation of oxygenated NMVOCs, which can be deposited to the surface [*Karl et al.,* 2010] or incorporated into particulate matter forming secondary organic aerosol [*Jimenez et al.,* 2009]. The oxidation of NMVOC creates a large pool of RO_2 and HO_2 radicals, which, in the presence of sufficient NO, can regenerate OH and form NO_2, and will consequently influence tropospheric ozone production [*Thornton et al.,* 2002]. Under conditions of low NO and high isoprene concentrations, the recycling of OH has been thought to become small so that the self-cleaning efficiency is greatly reduced in standard tropospheric chemistry schemes [*Lelieveld et al.,* 2008]. It has historically been a great challenge for Earth system models to simulate photochemistry when high isoprene emission fluxes occur in low NO_x environments (for example in tropical forests), typically leading to an overprediction of isoprene concentrations in the planetary boundary layer [*Karl et al.,* 2007]. Recent research on the atmospheric oxidation capacity in isoprene-dominated environments has suggested missing radical sources leading to significant overestimation of the lifetime of isoprene [*Carslaw et al.,* 2001; *Tan et al.,* 2001; *Thornton et al.,* 2002;

Lelieveld et al., 2008; *Ren et al.,* 2008; *Hofzumahaus et al.,* 2009; *Pugh et al.,* 2010; *Stone et al.,* 2011; *Whalley et al.,* 2011], with important ramifications for air quality and climate models [*Mao et al.,* 2012; *Fiore et al.,* 2011; *Knote et al.,* 2014].

In situ OH observations in pristine and polluted environments [*Lelieveld et al.,* 2008; *Ren et al.,* 2008; *Hofzumahaus et al.,* 2009] have indicated that traditional tropospheric chemical mechanisms likely miss a large portion of the recycling efficiency through unknown [*Lelieveld et al.,* 2008] or poorly quantified isoprene peroxy-radical reactions [*Hasson et al.,* 2004]. Subsequent work on isoprene oxidation schemes has identified various possibilities (see supporting information for more detail), with the isomerization of hydroxyl-peroxy radicals [*Peeters and Müller*, 2010] currently suggested to give the most plausible results [*Fuchs et al.,* 2013]. While it is established that OH is likely recycled more efficiently than previously thought, the exact mechanism and particularly the magnitude of this recycling remain a subject of debate [*Stone et al.,* 2011; *Fuchs et al.,* 2013; *Crounse et al.,* 2011]. Some conceptual modeling studies have pointed out that very high OH recycling rates could lead to an underestimation of isoprene concentrations in dynamically coupled chemistry models [*Vilà-Guerau de Arellano et al.,* 2011]. Slowing down the effective reaction rate of isoprene with OH due to incomplete mixing was proposed to mitigate this paradox [*Butler et al.,* 2008]. Theoretical studies using large eddy simulation (LES) showed that this slowdown of chemistry is most important when surface emissions are not uniform [*Krol et al.,* 2000; *Ouwersloot et al.,* 2011].

The Air Quality Modeling Evaluation International Initiative (phase 2) has recently identified regions with high isoprene abundance as particularly uncertain, producing the largest variability in predicted ozone [*Knote et al.,* 2014]. Since the sensitivity of tropospheric ozone production with respect to isoprene largely depends on an accurate representation of emissions and subsequent chemistry, knowing the atmospheric fate of isoprene serves as the primary constraint to assess uncertainties in modeling and observational approaches. The Southeast and Central U.S. have been important locations for studying the influence of biogenic volatile organic compounds on atmospheric chemistry for quite some time [*Chameides et al.,* 1988; *Trainer et al.,* 1987] and have recently received significant attention in biosphere-atmosphere exchange studies. Here we investigate the scale dependent effect of segregation between isoprene and OH and show that both mesoscale and microscale variability can cause an effective slowdown of isoprene due to incomplete mixing, which can be comparable to the effect of increased radical cycling [e.g., *Fuchs et al.,* 2013].

2. Theoretical Considerations

2.1. OH Calculation From the Total Isoprene Budget in the PBL

The budget equation of a trace gas in differential form after Reynolds decomposition is

$$\frac{\mathrm{d}\langle C\rangle}{\mathrm{d}t}+\frac{\mathrm{d}\langle w'c'\rangle}{\mathrm{d}z}+\langle u\rangle\frac{\mathrm{d}\langle C\rangle}{\mathrm{d}x}+\langle v\rangle\frac{\mathrm{d}\langle C\rangle}{\mathrm{d}y}=\langle Q_S\rangle \tag{1}$$

where the first term represents the storage component, the second term is the vertical flux divergence, and the third plus fourth terms represent horizontal advection. Brackets denote spatial averages along the flight leg, and primes denote the turbulent fluctuation of a quantity. In the above equation horizontal turbulent terms and vertical advection are already considered negligible components, an approach that has also been used for other trace gases [e.g., *Faloona et al.*, 2005]. For example, the mean subsidence rates measured during Nitrogen, Oxidants, Mercury and Aerosol Distributions, Sources and Sinks (NOMADSS) profiling flights were on the order of -0.09 ± 0.1 m/s, small ($<5\%$) compared to typical vertical wind velocity fluctuations. Left-hand side terms in equation (1) must balance all sources and sinks of the trace gas in the control volume. Q_S can be determined by the concentration of isoprene (C) divided by the lifetime $(\tau)\left(\langle Q_S\rangle := {}^{\langle C\rangle}/_{\tau}\right)$. The photochemical lifetime of isoprene is calculated according to

$$\tau=\frac{1}{k_{\mathrm{OH}}[\mathrm{OH}]+k_{\mathrm{O_3}}[\mathrm{O_3}]+k_{\mathrm{NO_3}}[\mathrm{NO_3}]}, \tag{2}$$

where k_{OH}, $k_{\mathrm{O_3}}$, and $k_{\mathrm{NO_3}}$ represent effective reaction rate constants for isoprene with respect to OH, ozone, and NO_3. For this study, contributions of ozone and NO_3 to the isoprene loss were small, of the order of $<10\%$ for O_3 (i.e., $\tau=14$–20 h) and $<1\%$ for NO_3 ($\tau>160$ h). Loss toward O_3 was calculated using average observed O_3 concentrations, and NO_3 concentrations were assumed <0.1 pptv as found in steady state calculations.

The photochemical lifetime of isoprene is therefore inversely proportional to the mean OH density in the PBL. Using measured values on the left-hand side of equation (1), it is possible to determine a lifetime for isoprene and subsequently OH densities.

2.2. Intensity of Segregation and Damköhler Number

The equation of the intensity of segregation can be derived from the scalar budget equation following Reynolds decomposition in a mean (denoted by <>) and fluctuating part (denoted by ′) (e. g., $[OH] = [\langle OH \rangle + OH']$). For a second-order species, I_s can then be derived according to equations (3)–(7)

$$\frac{\partial \langle [C_5H_8] \rangle}{\partial t} = \ldots - k \langle [OH][C_5H_8] \rangle \tag{3}$$

$$\frac{\partial \langle [C_5H_8] \rangle}{\partial t} = \ldots - k \left\langle \left[\langle OH \rangle + OH' \right] \left[\langle C_5H_8 \rangle + C_5H_8' \right] \right\rangle \tag{4}$$

$$\frac{\partial \langle [C_5H_8] \rangle}{\partial t} = \ldots - k \langle [OH] \rangle \langle [C_5H_8] \rangle - k \left\langle [OH]' [C_5H_8]' \right\rangle \tag{5}$$

$$\frac{\partial \langle [C_5H_8] \rangle}{\partial t} = \ldots - k \langle [OH] \rangle \langle [C_5H_8] \rangle \left(1 + \frac{\left\langle [OH]' [C_5H_8]' \right\rangle}{\langle [OH] \rangle \langle [C_5H_8] \rangle} \right) \tag{6}$$

$$I_S = \frac{\left\langle [OH]' [C_5H_8]' \right\rangle}{\langle [OH] \rangle \langle [C_5H_8] \rangle} \tag{7}$$

The numerator in equation (7) represents the covariance term between OH and isoprene fluctuations denoted by the primes. The effective reaction rate (k_{eff}) of a second-order reaction (e.g., Isoprene + OH − > Products) is then calculated as $k_{eff} = k(1 + I_s)$; thus if negative, the intensity of segregation directly translates to a slowdown of chemistry due to turbulent fluctuations. Positive I_s relates to correlated scalars increasing the speed of the reaction compared to completely well mixed conditions ($I_s = 0$).

The Damköhler number (Da) is a fundamental quantity in chemical engineering that relates the bulk chemical lifetime (e.g., $\tau_c = (k[OH])^{-1}$) to a transport time scale, here specified by the convective velocity scale (w^*) divided by the PBL height (z_i), where

$$\mathrm{Da} = \frac{z_i}{w^*} \frac{1}{\tau_c} \tag{8}$$

3. Experimental Methods

The Nitrogen, Oxidants, Mercury and Aerosol Distributions, Sources and Sinks (NOMADSS) project on the National Center for Atmospheric Research's C130 research aircraft was conducted under the umbrella of the Southeast Atmosphere Study. Within NOMADSS, the Southern Oxidant and Aerosol Study (SOAS) was one out of three projects. This paper focuses on results from SOAS. General information such as payload and experimental design of NOMADSS and SOAS can be found in summaries https://www.eol.ucar.edu/field_projects/nomadss. Nineteen research flights (RFs) were conducted in June/July 2013, some of which focused on isoprene emission hot spots in the southeast and central U.S. Figure S1(in the supporting information) shows the flight tracks overlaid on a map of isoprene emissions. To investigate the atmospheric fate of isoprene, we measured the complete planetary boundary layer (PBL) budget calculating eddy covariance fluxes during stacked racetracks flown at different heights within and above the PBL at key locations (Figure S1). The PBL height was obtained at each location by flux divergence profiles that were performed along with the horizontal transect flights [*Karl et al.,* 2013]. The PBL was then defined as the minimum of the sensible heat flux, alternatively as the lower level of the cumulus cloud layer, if present, identified from dew point temperature profiles and visual inspection of the cloud base layer during the research flight by the mission scientist. The variability of the PBLs during individual flights was largely caused by meteorological conditions. Particularly, RF04 and RF05 were subject to a large-scale disturbance causing significant cloud layers and rain events preceding the research flights. In addition, the OH chemical ionization mass spectrometer was not operational during these two flights, which are therefore excluded from the analysis of segregation.

Table 1. Racetrack Summary for Research Flights (RF) #13, #17, #05, and #04[a]

	RF13	RF17	RF05	RF04
Latitude	32.79°	37.25°	32.80°	32.79°
Longitude	−87.27°	−90.25°	−87.26°	−87.27°
Fs measured (mg/m^2/h)	5.3 ± 1.1	9.9 ± 2.1	5.5 ± 1.2	7.9 ± 1.7
Fs CLM-MEGAN (mg/m^2/h)	4.5 to 5.4	4.7 to 5.9	1.9 to 2.8	2.8 to 3.9
OH (flux) (molecules/cm^3)	$(2.9 \pm 0.4) \times 10^6$	$(3.6 \pm 0.5) \times 10^6$	$(6.6 \pm 0.9) \times 10^6$	$(2.8 \pm 0.4) \times 10^6$
OH [CIMS] (molecules/cm^3)	$(2.9 \pm 0.6) \times 10^6$	$(4.3 \pm 0.8) \times 10^6$	n/a	n/a
I_s	-13^{+4}_{-4}%	$-14^{+5.5}_{-5.5}$%	n/a	n/a
w^* (m/s)	1.4 ± 0.1	1.1 ± 0.1	0.9 ± 0.1	0.9 ± 0.1
Da	0.42	0.41	0.25	0.56
WDIR	49°	22°	20°	301°
U (m/s)	2.6 ± 1.1	5.9 ± 1.0	4.7 ± 1.1	4.0 ± 0.9
z_i (m)	2200 ± 100	1400 ± 100	950 ± 100	950 ± 100
v_e (cm/s)	<9.5	<5.3	<3.7	<3.1

[a]Listed are latitude and longitude of racetracks, isoprene surface fluxes Fs (measured and modeled from CLM-MEGAN), measured OH densities, intensity of segregation (I_s), convective velocity scale (w^*), Damköhler number (Da), wind direction (WDIR), wind speed (U), PBL height (z_i), and upper limits on entrainment velocities (v_e).

4. Results and Discussion

4.1. OH Comparison

During NOMADSS we are able to compare the PBL budget method [*Karl et al.,* 2013] with in situ OH measurements for the first time. After calculating storage, flux divergence, and advection, the left-hand terms of equation (1), OH concentrations within the PBL from the budget method were found between 2.8 and 6.6×10^6 molecules/cm^3 depending on research flight, day, and location (Table 1). Overlapping data for OH densities inferred from flux measurements and in situ instrumentation were available for research flights (RFs) 13 and 17 and are within 16% (Table 1), giving us confidence in the budget method.

From the same stacked racetrack flights boundary layer height (z_i), convective velocity scale (w^*), Damköhler numbers (Da), and upper limits on entrainment velocity (v_e) were calculated according to *Karl et al.* [2013] and are listed for the different flights in Table 1. Entrainment velocities calculated from isoprene flux gradients are sensitive to the estimation of the PBL height; therefore, lower PBL height estimates were used to calculate upper limits on entrainment velocities.

4.2. Measurements of the Intensity of Segregation

The intensity of segregation is calculated from the highly time resolved measurements of isoprene and OH according to equation (7). The covariance between OH fluctuations and isoprene fluctuations in the numerator is calculated using standard procedures for airborne VOC eddy covariance. Briefly, we deploy conventional fast Fourier transform (FFT) and wavelet analysis to investigate turbulent fluxes [*Karl et al.,* 2013]. Following general considerations [*Torrence and Compo*, 1998] and considering bias rectification [*Liu et al.,* 2007], we implemented a wavelet transformation routine using the Morlet wavelet. Two advantages of wavelet transforms include that (1) it does not rely on the ergodic hypothesis and therefore does not require stationarity, and (2) it allows investigating time resolved spectral contributions to the measured flux. Integrated cospectra (i.e., fluxes) typically agreed to within ± 10% between FFT and wavelet transforms for the profiling flights. Figure S3 shows a typical example of a normalized cospectrum for sensible heat and isoprene using conventional FFT for RF17. It should be noted that the spectral analysis of VOC data is limited to the Nyquist frequency imposed by a disjunct sampling interval of 1 s; during NOMADSS, this cutoff frequency resulted in a spectral loss of less than 5%. OH measurements have a time resolution of 30 s (green line in Figure S3). While OH measurements during NOMADSS were obtained at a relatively slow sampling rate, we used spectral similarity considerations to reconstruct the spectral high-frequency loss based on concomitant fast isoprene and ozone measurements available up to 5 Hz sampling rate (Figure S4).

Figure 1 shows a typical wavelet plot of the effect of segregation. Based on typical cospectra (Figure S3), we define any contribution to the covariance at time scales greater than 250 s (lower than 5×10^{-3} Hz, approximately > 25 km) as mesoscale. The cospectra between both OH and O_3 with isoprene suggest that mesoscale

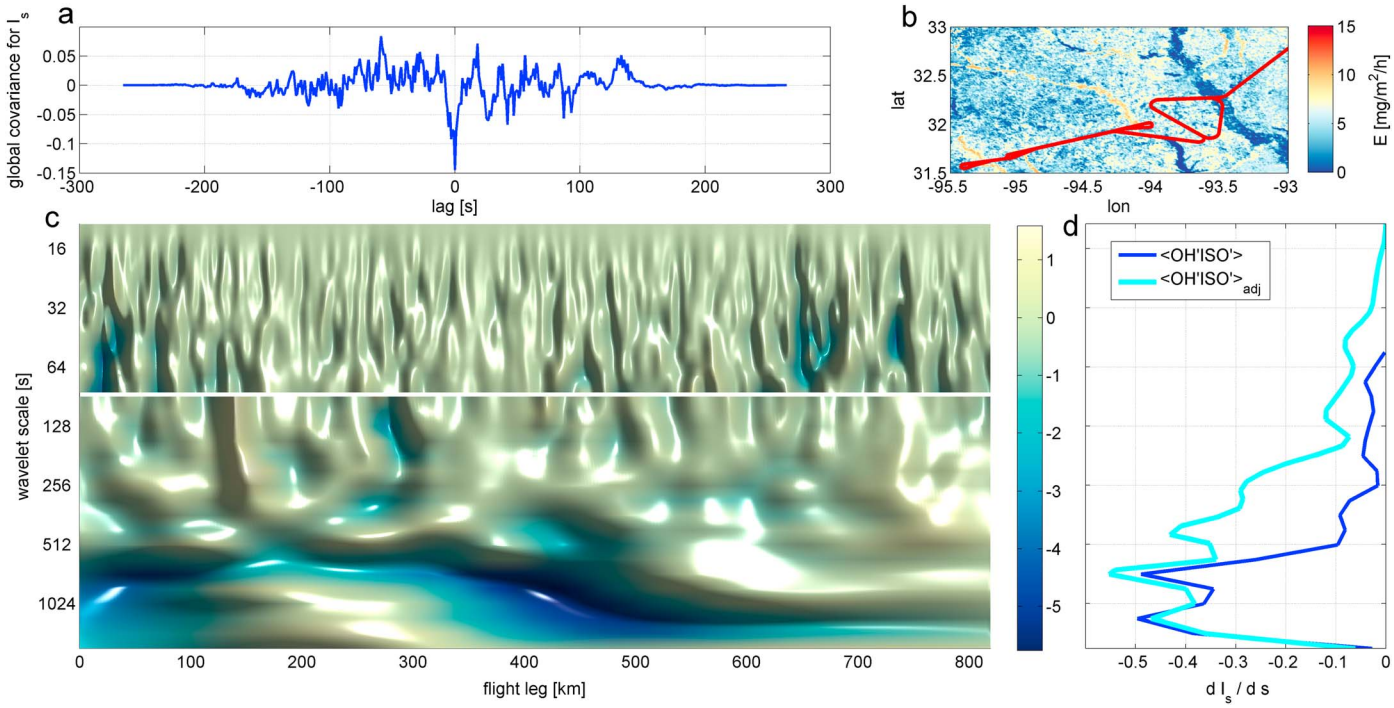

Figure 1. Correlation analysis of the Intensity of segregation. (a) Global covariance for $I_s = \frac{\langle [OH]'[C_5H_8]' \rangle}{\langle [OH] \rangle \langle [C_5H_8] \rangle}$. (b) Flight track (lat: latitude; lon: longitude) on top of isoprene emission map. (c) Dimensionless wavelet cross spectrum calculated for $\langle [O_3]'[C_5H_8]' \rangle$ (below wavelet scale of 78 s) and $\langle [OH]'[C_5H_8]' \rangle$ (for wavelet scale >80 s). (d) Global wavelet spectrum for dI_s/ds as a function of wavelet scale [s] (*y* axis is the same as in Figure 1c). The light blue line represents the adjusted wavelet spectrum for $\langle [OH]'[C_5H_8]' \rangle$ after spectral attenuation corrections to the raw data (blue line) as described in the text.

variations induced by surface heterogeneity can play an important role in producing segregation effects and that even at the smallest scales the segregation can be significant. As an example, Figure 1 shows clear local minima of I_s at wavelet scales between 500 and 1000 s during research flight (RF) 13. At typical aircraft speeds, these large-scale features would correspond to spatial scales on the order of 50–100 km and exhibit local I_s of −19%. During RF17, local segregation was measured as large as −30%. The data suggest that surface heterogeneity larger than typical PBL scales can contribute a significant fraction to the intensity of segregation, which are likely not resolved in models similar to the ones used by *Lelieveld et al.* [2008]. In total, we obtained six independent and representative PBL values for I_s during two research flights above forested regions in the SE (including the Ozarks) averaging to -13^{+6}_{-7}%, where about half of the total (−6 to −8%) is caused by the smallest scales of motion ($>5 \times 10^{-3}$ Hz).

Values for the intensity of segregation in the roughness sublayer of a forest [*Dlugi et al.*, 2010; *Pugh et al.*, 2011], where segregation effects are predicted to be significantly larger than in the PBL [*Patton et al.*, 2001], were reported to lie between −1 and −10%. *Butler et al.* [2008], on the other hand, estimated an average PBL value for I_s of −13% over the Guyanas and speculated it was a lower limit due to high-frequency damping in their measurements. They argued that a PBL average for I_s up to −50% would be necessary to produce good agreement for isoprene concentrations between model and measurements. In contrast, a different modeling study [*Verver et al.*, 2000] reported values for I_s that were 50 times smaller than those of *Butler et al.* [2008] along with Da numbers for isoprene of only 0.02 during midday conditions. Based on large eddy simulation (LES) models [*Patton et al.*, 2001; *Vinuesa and Vilà-Guerau de Arellano*, 2003], a range of I_s between −5% (Da = 0.17) [*Patton et al.*, 2003] to −17% (Da = 0.6) [*Vinuesa and Vilà-Guerau de Arellano*, 2003] was predicted previously for homogenous land cover. The model to model variability is expected due to differences in (1) flow regimes (e.g., neutral vs unstable stratification and the resultant evolution of turbulence space and time scales), (2) domain size (also affecting the mixing time of the largest scales of turbulence), (3) inclusion of a plant canopy, and (4) model resolution (e.g., subgrid scale model parameterization). The average during NOMADSS $\left(I_s = -13^{+6}_{-7}\%\right)$ and the upper range observed over heterogeneous land surface transitions

($I_s = -20$ to -30%) suggest significantly lower numbers for I_s and larger values for Da than some of the previous model estimates [*Patton et al.,* 2001; *Ververt et al.,* 2000]. Da numbers for isoprene $\left(0.41^{+0.15}_{-0.16}\right)$ observed during NOMADSS are comparable to values reported above an oak forest in California $\left(\mathrm{Da} = 0.50^{+0.4}_{-0.3}\right)$ [*Karl et al.,* 2013]. We speculate that the smaller Da numbers in some of the earlier model simulations could be partly due to missing radical cycling and a lower degree of heterogeneity of isoprene emissions; this is to some extent supported by wavelet analysis showing highly segregated air masses in the PBL air at scales associated with mesoscale variability that also influence isoprene concentrations. In transitional areas going from high to low isoprene emission environments, I_s was observed as low as -30%. Isoprene fluxes were positively correlated with sensible heat fluxes ($R = 0.42$) and exhibited a negative correlation with I_s ($R = 0.33$) (see Figures S5 and S6). These correlations along with the above presented wavelet analysis point at a feedback loop—the higher the isoprene flux the larger the I_s. This could lead to an underestimation of OH due to limited spatial resolution. The findings are corroborated by a set of canopy-resolving large eddy simulations investigating the effect of surface emission heterogeneity (Text S7 and Figures S10 and S11) that could induce additional segregation effects, adding up to -20% in the PBL and -55% inside of a plant canopy. In contrast, segregation effects between ozone and different NO_x species were expectedly small (e.g., I_s ($NO + O_3$) $< 1\%$).

4.3. Observed and Modeled Isoprene Fluxes

Detailed flux profile measurements [e.g., *Karl et al.,* 2013] were obtained from the same four profiling flights listed in Table 1, which compares measured isoprene surface fluxes with isoprene emissions from the implementation of Model of Emissions of Gases and Aerosols from Nature version 2.1. (MEGAN-v2.1) in the Community Land Model (CLM; for details, see Text S5). For the four locations investigated, we find an emission model/measurement ratio of 0.4 ± 0.3 to 0.9 ± 0.3 for CLM-MEGAN. Significant uncertainties of isoprene emissions in the model are associated with the attribution of emission factors to different land cover types, where surface heterogeneity introduces substantial variability [*Guenther et al.,* 2006]. The variability in measurement-model comparisons suggests land surface heterogeneity as one of the largest uncertainties inherent to regional biogenic emission estimates. This can have important ramifications on the physical separation of reactants.

In order to investigate the influence of land surface heterogeneity within the above mentioned uncertainty, we performed a spectral decomposition of isoprene emission factors based on land surface data implemented in MEGAN-v2.1 (2 km grid) along individual flight tracks. Figure 2 shows such an example for RF13 that is discussed in detail in Figure 1. The *x* axis in Figure 2 depicts a normalized length scale that we define as the horizontal scale (λ) divided by the PBL height (z_i) during the research flight. The *y* axis shows the spectral contribution to the isoprene emission factor variability. Vertical lines show length scales associated with PBL turbulence (red), scales investigated by *Ouwersloot et al.* [2011] (black) and a typical grid resolution of 2.8° (based on a T42 grid) (green) used in some global 3-D models [e.g., *Lelieveld et al.,* 2008]. It can be seen that the large mesoscale feature on time scales between 500 and 1000 s, which we also obtain by the wavelet analysis of I_s (Figure 1), corresponds well to the major contribution of the isoprene emission factor variability. The variability on horizontal scales $\lambda/z_i = 10$–100 can contribute about 4 times as much to the overall variability than scales investigated by *Ouwersloot et al.* [2011]. It is noted that none of the shown variability of isoprene emissions would be represented on a T42 grid and would therefore be missed. A first quantitative assessment of this effect can be gained from the correlation plot between I_s and isoprene fluxes (Figure S6). I_s exhibits a negative correlation with isoprene fluxes. This behavior was observed for all flights and suggests that, during NOMADSS, the production of covariance (i.e.. $<[\mathrm{OH}]'\,[\mathrm{C_5H_8}]'>$) is generally dependent on the magnitude of the isoprene flux. This behavior can be rationalized by comparing with the budget equation for the covariance as has been outlined, for example, by *Vinuesa and Vilà-Guerau de Arellano* [2003]. Here in the case of Isoprene and OH, we can define the production of covariance as

$$\frac{\partial\left\langle [\mathrm{C_5H_8}]'[\mathrm{OH}]'\right\rangle}{\partial t} = -\left\langle w'[\mathrm{C_5H_8}]'\right\rangle \frac{\partial\langle[\mathrm{OH}]\rangle}{\partial z} - \left\langle w'[\mathrm{OH}]'\right\rangle \frac{\partial\langle[\mathrm{C_5H_8}]\rangle}{\partial z} - T - D - R_{\mathrm{C_5H_8,OH}}, \tag{9}$$

where the left-hand side represents the change of the covariance between OH and isoprene which is directly proportional to I_s. The first two terms on the right-hand side are the flux gradient terms. *T*, *D*, and *R* are the turbulent transport, dissipation, and chemical terms.

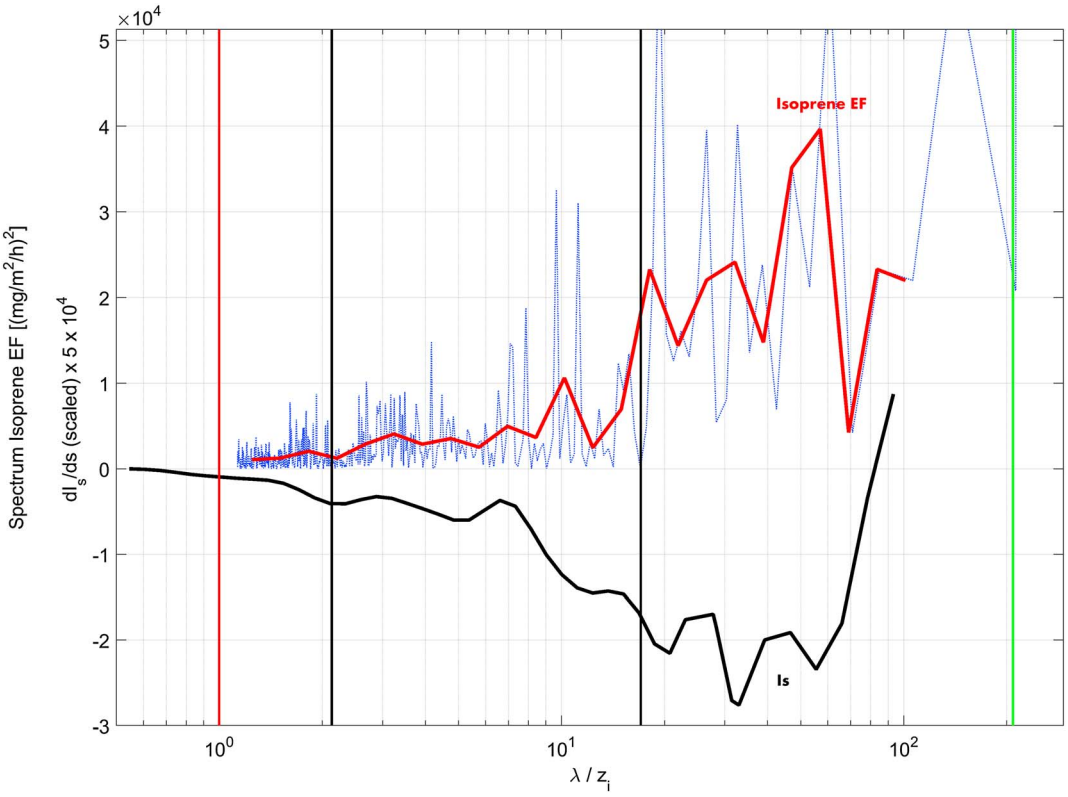

Figure 2. Statistics of isoprene emission factors along flight track R13 depicted in Figure 1: Spectral decomposition (dotted blue: raw; thick red: decadal average) of isoprene emission factors. Replotted from Figure 1 is the corrected intensity of segregation (I_s). Typical length scales are depicted by vertical lines (red: PBL scales, black: range investigated by *Ouwersloot et al.*, 2011; green: T42 grid).

The gradient terms (1 and 2 on the right side) reduce to the first term because OH is not transported ($<w'OH'> = 0$). The isoprene flux is positive and d[OH]/dz is generally positive as OH increases with z (verified by NOMADSS measurements). Thus, an increase in isoprene flux should lead to an enhanced production of I_s as observed in the real data sets.

We further investigated the impact of I_s on modeled OH using constrained box models.

4.4. Impact on Predicted OH

Previous work [e.g., *Wolfe and Thornton*, 2011] has demonstrated the complexity of a fully coupled 1-D chemistry simulation above a Californian forest using the Leeds Master Chemical Mechanism (MCMv3.1). In order to simplify the interpretation, we investigate the relative magnitude of slower chemistry on OH based on a constrained box modeling analysis in a Lagrangian sense similar to *Olson et al.* [2006]. Details about the measurements constraining the box model, the chemical mechanisms (MCMv3.2), and what OH recycling schemes were implemented are given in Texts S1–S4 and S6 and in Tables S1 and S2. A detailed comparison between modeled and measured HO_x species is shown in Figure S8. Overall, modeled HO_2 lies within the measurement uncertainty of observed HO_2 (±35% for values well above 2 pptv) for all simulations (MCMv3.2). Modeled OH is underpredicted during RF17 by 47%, during RF13 the MCM underpredicts OH by only 15%. Figure S9 shows the most dominant chemical production and loss terms in the OH budget. The combination of higher primary production and secondary recycling via NO, together with a lower isoprene sink and lower measured OH during RF13, likely plays a key role that we can close the OH mismatch better for RF13 than for RF17.

On average, segregation has an effect on modeled OH that is similar to the recently proposed adjusted LIM2010-J recycling mechanism [*Fuchs et al.*, 2013] (Figure 3). Adding recently suggested recycling mechanisms and a 13% reduction of the isoprene + OH rate constant to the MCM code increases the modeled OH by

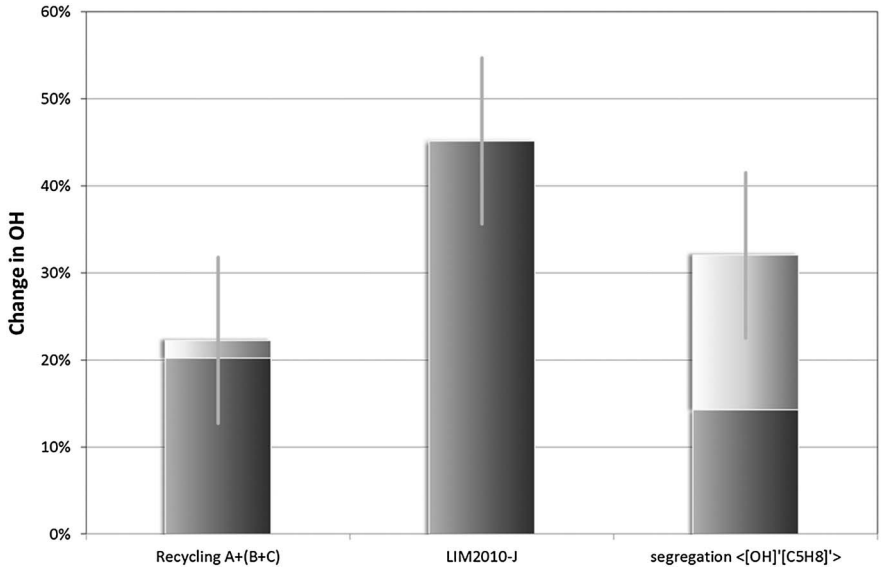

Figure 3. Influence on modeled OH (average for RF13 and RF17) expressed as a relative contribution to the total change 100%) based on the following mechanistic modifications: Recycling A+(B + C) (a total of three recently proposed recycling mechanisms (B + C) are added together and contribute equally to the light-shaded area; see definition of A, B, and C in Table S1), LIM2010-J (recently modified Leuven recycling mechanism, see Table S1), and segregation effects (light shaded: mesoscale contribution). Error bars indicate systematic uncertainty based on the intercomparison of isoprene measurements (Figure S2).

about 24%. Together, these two mechanistic changes (recycling and segregation) have the largest effect on modeled OH and would reconcile modeled to measured OH to within 88^{+20}_{-20}%. The differences in modeled and measured OH in this study are similar to recently reported chamber measurements [*Fuchs et al.,* 2013] and much smaller than values published for previous field studies [*Lelieveld et al.,* 2008; *Hofzumahaus et al.,* 2009; *Stone et al.,* 2011; *Whalley et al.,* 2011]. Notably, *Stone et al.* [2010] reported no significant missing HO_x source during the African Monsoon Multidisciplinary Analyses field experiment, when comparing to a lumped chemical scheme. While isoprene concentrations were somewhat higher during NOMADSS, the NO_x and ozone environment were comparable between these two studies. Mean NO levels during the NOMADSS RF13 and RF17 flights were 63 pptv and 46 pptv, respectively (average concentrations of other trace gases during the investigated flights are given in Table S2). The measurements also show that segregation can slow down chemistry by as much as 30% in the PBL, depending on surface heterogeneity. The potential of such a large change is supported by canopy-resolving large eddy simulations (LES) (Figure S11) and is an important consideration for the interpretation of radical cycling in mesoscale and synoptic scale atmospheric chemistry models. In such cases, the effect of segregation could potentially dominate the effects on predicted local OH densities.

5. Summary and Conclusions

Chemistry-turbulence interaction terms appearing in the Reynolds-averaged Navier Stokes equations used in 3-D chemistry transport models (CTM)—and which are typically ignored—can significantly modify the atmospheric oxidation efficiency. They have an influence on the lifetime of isoprene in the forested PBL that is comparable to recently proposed chemical oxidant recycling mechanisms. Reactive trace gases such as isoprene are particularly prone to chemistry-turbulence interactions due to a comparable chemical lifetime with respect to the mixing time scale (Da = 0.4–1). Our measurements demonstrate that the overall effect of segregation depends on (1) chemistry-turbulence interactions and (2) scale dependent heterogeneity of isoprene emissions. We find that even for horizontally homogeneous PBL motions, emission heterogeneity can induce segregation and alter reaction rates. The combined effect in CTMs likely varies depending on each modeling framework; our measurements show that segregation's influence in large-scale models will, to a large extent, depend on the ability to characterize surface heterogeneity and associated variability. A

more accurate representation of the spatial variability of isoprene emissions in models should therefore reduce the uncertainty of predicted OH in the PBL. The presented data provide a realistic range of the magnitude of chemistry-turbulence interactions in the PBL. We conclude that airborne flux measurements are a useful experimental technique to disentangle these complex interactions on the cycling of reactive gases in the atmosphere.

Acknowledgments
We thank the NCAR EOL flight crew and the NOMADSS science team for excellent mission support. We are grateful to T. Campos for collecting and supplying CO and methane data. The National Center for Atmospheric Research is operated by the University Cooperation for Atmospheric Research and is sponsored by the National Science Foundation. Data are provided by NCAR/EOL under sponsorship of the National Science Foundation. T.K. was also supported by the EC Seventh Framework Program (Marie Curie Reintegration Program, "ALP-AIR", grant 334084). C.A.C. and R.L.M. were supported by NSF grant 1216743.

References

Butler, T. M., D. Taraborrelli, C. Brühl, H. Fischer, H. Harder, M. Martinez, J. Williams, M. G. Lawrence, and J. Lelieveld (2008), Improved simulation of isoprene oxidation chemistry with the ECHAM5/MESSy chemistry-climate model: Lessons from the GABRIEL airborne field campaign, *Atmos. Chem. Phys.*, *8*, 4529–4546, doi:10.5194/acp-8-4529-2008.

Carslaw, N., et al. (2001), OH and HO_2 radical chemistry in a forested region of north-western Greece, *Atmos. Environ.*, *35*, 4725–4737, doi:10.1016/S1352-2310(01)00089-9.

Chameides, W., R. W. Lindsay, J. Richardson, and C. S. Kiang (1988), The role of biogenic hydrocarbons in urban photochemical smog: Atlanta as a case study, *Science*, *241*(4872), 1473–1475, doi:10.1126/science.3420404.

Crounse, J. D., F. Paulot, H. G. Kjaergaard, and P. O. Wennberg (2011), Peroxy radical isomerization in the oxidation of isoprene, *Phys. Chem. Chem. Phys.*, *13*, 13,607–13,613, doi:10.1039/C1CP21330J.

Dlugi, R., et al. (2010), Turbulent exchange and segregation of HO_x radicals and volatile organic compounds above a deciduous forest, *Atmos. Chem. Phys.*, *10*, 6215–6235, doi:10.5194/acp-10-6215-2010.

Faloona, I., D. H. Lenschow, T. Campos, B. Stevens, M. van Zanten, B. Blomquist, D. Thornton, A. Bandy, and H. Gerber (2005), Observations of entrainment in eastern Pacific marine stratocumulus using three conserved scalar, *J. Atmos. Sci.*, *62*, 3268–3285, doi:10.1175/JAS3541.1.

Fiore, A. M., H. Levy II, and D. A. Jaffe (2011), North American isoprene influence on intercontinental ozone pollution, *Atmos. Chem. Phys.*, *11*, 1697–1710, doi:10.5194/acp-11-1697-2011.

Fuchs, H., et al. (2013), Experimental evidence for efficient hydroxyl radical regeneration in isoprene oxidation, *Nat. Geosci.*, *6*, 1023–1026, doi:10.1038/ngeo1964.

Goldstein, A. H., and I. Galbally (2007), Known and unexplored organic constituents in the Earth's atmosphere, *Environ. Sci. Technol.*, *41*, 1515–1521, doi:10.1021/es072476p.

Guenther, A., T. Karl, P. Harley, C. Wiedinmyer, P. I. Palmer, and C. Geron (2006), Estimates of global terrestrial isoprene emissions using MEGAN (Model of Emissions of Gases and Aerosols from Nature), *Atmos. Chem. Phys.*, *6*, 3181–3210, doi:10.5194/acp-6-3181-2006.

Hasson, A. S., G. S. Tyndall, and J. J. Orlando (2004), A product yield study of the reaction of HO_2 radicals with ethyl peroxy ($C_2H_5O_2$) acetyl peroxy ($CH_3C(O)O_2$), and acetonyl peroxy ($CH_3C(O)CH_2O_2$) radicals, *J. Phys. Chem.*, *108*, 5979–5989, doi:10.1021/jp048873t.

Hofzumahaus, A., et al. (2009), Amplified trace gas removal in the troposphere, *Science*, *324*, 1702–1704, doi:10.1126/science.1164566.

Jimenez, J. L., et al. (2009), Evolution of organic aerosol in the atmosphere, *Science*, *326*, 1525–1529, doi:10.1126/science.1180353.

Karl, T., A. Guenther, R. J. Yokelson, J. Greenberg, M. Potosnak, D. R. Blake, and P. Artaxo (2007), The tropical forest and fire emissions experiment: Emission, chemistry, and transport of biogenic volatile organic compounds in the lower atmosphere over Amazonia, *J. Geophys. Res.*, *112*, D18302, doi:10.1029/2007JD008539.

Karl, T., P. Harley, L. Emmons, B. Thornton, A. Guenther, C. Basu, A. Turnipseed, and K. Jardine (2010), Efficient atmospheric cleansing of oxidized organic trace gases by vegetation, *Science*, *330*, 816–819, doi:10.1126/science.1192534.

Karl, T., P. K. Misztal, H. H. Jonsson, S. Shertz, A. H. Goldstein, and A. B. Guenther (2013), Airborne flux measurements of BVOCs above Californian oak forests: Experimental investigation of surface and entrainment fluxes, OH densities, and Damkohler numbers, *J. Atmos. Sci.*, *70*, 3277–3287, doi:10.1175/JAS-D-13-054.1.

Knote, C., et al. (2014), Influence of the choice of gas-phase mechanism on predictions of key gaseous pollutants during the AQMEII phase-2 intercomparison, *Atmos. Environ.*, *115*, 553–568, doi:10.1016/j.atmosenv.2014.11.066.

Krol, M. C., M. J. Molemaker, and J. de Vilu-Guerau (2000), Effects of turbulence and heterogeneous emissions on photochemical active species in the convective boundary layer, *J. Geophys. Res.*, *105*, 6871–6884, doi:10.1029/1999JD900958.

Lelieveld, J., et al. (2008), Atmospheric oxidation capacity sustained by a tropical forest, *Nature*, *452*, 737–740, doi:10.1038/nature06870.

Liu, Y., X. S. Liang, and R. H. Weisberg (2007), Rectification of the bias in the wavelet power spectrum, *J. Atmos. Oceanic Technol.*, *24*, 2093–2102, doi:10.1175/2007JTECHO511.1.

Loreto, F., M. Dicke, J.-P. Schnitzler, and T. C. J. Turlings (2014), Plant volatiles and the environment, *Plant, Cell Environ.*, *37*, 1905–1908, doi:10.1111/pce.12369.

Mao, J., et al. (2012), Insights into hydroxyl measurements and atmospheric oxidation in a California forest, *Atmos. Chem. Phys.*, *12*, 8009–8020, doi:10.5194/acp-12-8009-2012.

Olson, J. R., J. H. Crawford, G. Chen, W. H. Brune, I. C. Faloona, D. Tan, H. Harder, and M. Martinez (2006), A reevaluation of airborne HO_x observations from NASA field campaigns, *J. Geophys. Res.*, *111*, D10301, doi:10.1029/2005JD006617.

Ouwersloot, H. G., J. Vilà-Guerau de Arellano, C. C. van Heerwaarden, L. N. Ganzeveld, M. C. Krol, and J. Lelieveld (2011), On the segregation of chemical species in a clear boundary layer over heterogeneous land surfaces, *Atmos. Chem. Phys.*, *11*, 10,681–10,704, doi:10.5194/acp-11-10681-2011.

Patton, E. G., K. J. Davis, M. C. Barth, and P. P. Sullivan (2001), Decaying scalars emitted by a forest canopy: A numerical study, *Boundary Layer Meteorol.*, *100*, 91–129, doi:10.1023/A:1019223515444.

Patton, E. G., P. P. Sullican, and K. J. Davis (2003), The influence of a forest canopy on top-down and bottom-up diffusion in the planetary boundary layer, *Q. J. R. Meteorol. Soc.*, *129*, 1415–1434, doi:10.1256/qj.01.175.

Peeters, J., and J.-F. Müller (2010), HO_x radical regeneration in isoprene oxidation via peroxy radical isomerisations. II: Experimental evidence and global impact, *Phys. Chem. Chem. Phys.*, *12*, 14,227–14,235, doi:10.1039/C0CP00811G.

Pugh, T. A. M., et al. (2010), Simulating atmospheric composition over a South-East Asian tropical rainforest: Performance of a chemistry box model, *Atmos. Chem. Phys.*, *10*, 279–298, doi:10.5194/acp-10-279-2010.

Pugh, T. A. M., A. R. MacKenzie, B. Langford, E. Nemitz, P. K. Misztal, and C. N. Hewitt (2011), The influence of small scale variations in isoprene concentrations on atmospheric chemistry over a tropical rainforest, *Atmos. Chem. Phys.*, *11*, 4121–4134, doi:10.5194/acp-11-4121-2011.

Ren, X., et al. (2008), HO_x chemistry during INTEX-A 2004: Observation, model calculation, and comparison with previous studies, *J. Geophys. Res.*, *113*, D05310, doi:10.1029/2007JD009166.

Stone, D., et al. (2010), HO_x observations over West Africa during AMMA: Impact of isoprene and NO_x, *Atmos. Chem. Phys.*, *10*, 9415–9429, doi:10.5194/acp-10-9415-2010.

Stone, D., et al. (2011), Isoprene oxidation mechanisms: Measurements and modelling of OH and HO_2 over a South-East Asian tropical rainforest during the OP3 field campaign, *Atmos. Chem. Phys.*, *11*, 6749–6771, doi:10.5194/acp-11-6749-2011.

Tan, D., et al. (2001), HO_x budget in a deciduous forest: Results from the PROPHET summer 1998 campaign, *J. Geophys. Res.*, *106*, 24,407–24,427, doi:10.1029/2001JD900016.

Thornton, J. A., et al. (2002), Ozone production rates as a function of NO_x abundances and HO_x production rates in the Nashville urban plume, *J. Geophys. Res.*, *107*(D12), 4146, doi:10.1029/2001JD000932.

Torrence, C., and G. P. Compo (1998), A practical guide to wavelet analysis, *Bull. Am. Meteorol. Soc.*, *79*, 61–78, doi:10.1175/1520-0477(1998)079<0061:APGTWA>2.0.CO;2.

Trainer, M., E. J. Williams, D. D. Parrish, M. P. Buhr, E. J. Allwine, H. H. Westberg, F. C. Fehsenfeld, and S. C. Liu (1987), Models and observations of the impact of natural hydrocarbons on rural ozone, *Nature*, *329*, 705–707, doi:10.1038/329705a0.

Verver, G. H. L., H. van Dop, and A. A. M. Holtslag (2000), Turbulent mixing and the chemical breakdown of isoprene in the atmospheric boundary layer, *J. Geophys. Res.*, *105*, 3983–4002, doi:10.1029/1999JD900956.

Vilà-Guerau de Arellano, J., E. G. Patton, T. Karl, K. van den Dries, M. C. Barth, and J. J. Orlando (2011), The role of boundary layer dynamics on the diurnal evolution of isoprene and the hydroxyl radical over tropical forests, *J. Geophys. Res.*, *116*, D07304, doi:10.1029/2010JD014857.

Vinuesa, J.-F., and J. Vilà-Guerau de Arellano (2003), Fluxes and (co-)variances of reacting scalars in the convective boundary layer, *Tellus, Ser. B*, *55*, 935–949.

Whalley, L. K., et al. (2011), Quantifying the magnitude of a missing hydroxyl radical source in a tropical rainforest, *Atmos. Chem. Phys.*, *11*, 7223–7233, doi:10.5194/acp-11-7223-2011.

Wolfe, G. M., and J. A. Thornton (2011), The Chemistry of Atmosphere-Forest Exchange (CAFE) model—Part 1: Model description and characterization, *Atmos. Chem. Phys.*, *11*, 77–101, doi:10.5194/acp-11-77-2011.